The heterogeneous motility of the Lyme disease spirochete in gelatin mimics dissemination through tissue

Michael W. Harman[a,b], Star M. Dunham-Ems[a], Melissa J. Caimano[a], Alexia A. Belperron[c], Linda K. Bockenstedt[c], Henry C. Fu[d], Justin D. Radolf[a], and Charles W. Wolgemuth[b,1]

[a]Departments of Medicine, Pediatrics, Genetics and Developmental Biology, and Immunology, University of Connecticut Health Center, Farmington, CT 06030-3715; [b]Department of Cell Biology and Center for Cell Analysis and Modeling, University of Connecticut Health Center, Farmington, CT 06030-6406; [c]Department of Internal Medicine, Yale University, New Haven, CT 06520-8031; and [d]Department of Mechanical Engineering, University of Nevada, Reno, NV 89509

Edited* by Charles S. Peskin, New York University, New York, NY, and approved January 10, 2012 (received for review September 5, 2011)

The Lyme disease spirochete *Borrelia burgdorferi* exists in nature in an enzootic cycle that involves the arthropod vector *Ixodes scapularis* and mammalian reservoirs. To disseminate within and between these hosts, spirochetes must migrate through complex, polymeric environments such as the basement membrane of the tick midgut and the dermis of the mammal. To date, most research on the motility of *B. burgdorferi* has been done in media that do not resemble the tissue milieus that *B. burgdorferi* encounter in vivo. Here we show that the motility of *Borrelia* in gelatin matrices in vitro resembles the pathogen's movements in the chronically infected mouse dermis imaged by intravital microscopy. More specifically, *B. burgdorferi* motility in mouse dermis and gelatin is heterogeneous, with the bacteria transitioning between at least three different motility states that depend on transient adhesions to the matrix. We also show that *B. burgdorferi* is able to penetrate matrices with pore sizes much smaller than the diameter of the bacterium. We find a complex relationship between the swimming behavior of *B. burgdorferi* and the rheological properties of the gelatin, which cannot be accounted for by recent theoretical predictions for microorganism swimming in gels. Our results also emphasize the importance of considering borrelial adhesion as a dynamic rather than a static process.

The movements of microorganisms have fascinated researchers for >300 y, yet we are still just beginning to understand many aspects of these movements. As a prime example, the swimming of cells and microorganisms is almost universally driven by the undulation or rotation of thin filaments, whether it be the flapping of eukaryotic flagella, the beating of cilia, or the spinning of bacterial flagella (1). A baseline understanding of how these motions produce the thrust to propel a microorganism through water was developed by the pioneering work of G. I. Taylor and E. M. Purcell (2–4). In their natural environments, though, many microorganisms move through substances that do not behave like water. The nematode *Caenorhabditis elegans* lives in soil and undulates its body to move (5). In addition to soil, the nematode can move through viscous and viscoelastic fluids and gels and along the top of moist surfaces using similar undulatory motions (6). *C. elegans* changes its gait depending on the viscosity of the environment (6); viscoelasticity in the environment slows the swimming speed (7). Changes in the wave shape and frequency of the beating flagellum may enhance the ability of mammalian sperm to move through viscoelastic fluids, such as cervical mucus (8). Recent theoretical work has tried to explain how viscoelastic or gel-like media affect the swimming of microorganisms (9–14), but, to date, there have been very few empirical studies to test the theoretical predictions (7).

Here we focus on the spirochete that causes Lyme disease, *Borrelia burgdorferi* (*Bb*), which traverses complex environments during its enzootic cycle. The motility of *Bb* has been studied extensively in liquid media and methylcellulose solutions (see, for instance, ref. 15). Like most other swimming bacteria, *Bb* moves through these environments by rotating long, helical flagellar filaments. However, in spirochetes, the flagella are enclosed within the periplasmic space, the narrow region between the cell wall (i.e., cytoplasmic membrane plus peptidoglycan layer) and the outer membrane (16). The flagella are attached to 7–11 motor complexes positioned near the ends of the microorganism (17). The filaments originating from each end wrap around the cell body and are often long enough to overlap in the center of the bacterium (16). Forces between the cell cylinder and the flagella cause the cell body to deform into a planar, wave-like shape (18). When the flagella rotate, the cell body undulates as a traveling waveform (19), which drives the swimming of the bacterium.

Liquid media and methylcellulose solutions, though, are poor facsimiles for many of the environments that *Bb* encounter in nature. Lyme disease spirochetes transition between two markedly different hosts, the arthropod vector *Ixodes scapularis* and small mammals, such as *Peromyscus leucopus*, the white-footed mouse (20). To move from the tick to the mammal, *Bb* must migrate through many different tissues. In the tick, a small number of spirochetes exit the midgut during feeding by traversing a layer of epithelial cells and a thin, but dense, polymeric network known as a basement membrane (21). The spirochetes then swim through the hemocoel, a fluid environment containing hemocytes and hemolymph, where they attach to the salivary glands, penetrate another basement membrane, and enter the salivary ducts (22). *Bb* is then inoculated into the skin of its mammalian host where it translocates through the collagen-dense extracellular matrix (ECM) to access small vessels that provide portals for hematogenous dissemination. Cultured spirochetes injected i.v. into the vasculature undergo transient and dragging interactions before attaching firmly to the microvascular endothelium and working their way through interjunctional spaces separating endothelial cells (23). The tissue barriers that *Bb* navigates in ticks and mammals respond with a combination of viscous and elastic behavior to forces generated by the bacterium. These natural environments are differentiated further from liquid media and methylcellulose solutions because they contain cells and various ECM components, such as collagen, fibronectin, and decorin, to which *Bb* binds (24). How adhesion influences microorganism motility has not been explored from an experimental or theoretical perspective.

To begin to understand the motility of *Bb* in its natural environments, here we use gelatin matrices to bridge the gap

Author contributions: M.W.H., S.M.D.-E., M.J.C., A.A.B., L.K.B., J.D.R., and C.W.W. designed research; M.W.H., S.M.D.-E., A.A.B., and L.K.B. performed research; C.W.W. contributed new reagents/analytic tools; M.W.H., H.C.F., and C.W.W. analyzed data; and M.W.H., S.M.D.-E., L.K.B., J.D.R., and C.W.W. wrote the paper.

The authors declare no conflict of interest.

*This Direct Submission article had a prearranged editor.

[1]To whom correspondence should be addressed. E-mail: cwolgemuth@uchc.edu.

This article contains supporting information online at www.pnas.org/lookup/suppl/doi:10.1073/pnas.1114362109/-/DCSupplemental.

between controllable, in vitro motility assays and the natural environments that *Bb* encounters. Gelatin, a denatured form of collagen, was chosen because it possesses many of the same binding sites as native collagen (25) and because it has been used as an in vitro equivalent to the ECM for the study of borrelial motility (21, 26). We find that *Bb* in the dermis of chronically infected mice and in gelatin exhibit three or four motility states, which are determined by transient adhesion between the bacterium and the matrix. In addition to adhering to these substrates, spirochetes can migrate through them, even though the pores in the gelatin matrices are significantly smaller than the diameter of the bacteria. The undulation and migration speed of the bacteria are found to depend strongly on the physical properties of the environment. This work shows that gelatin is a good facsimile for the ECM and reveals the biophysical effects of the environment on borrelial motility. In addition, we deduce that adhesion is a dynamic process that allows *Bb* to transition between stationary and migratory behaviors.

Results

***B. burgdorferi* Motility in the Mouse Dermis Includes Motility States Not Observed in Liquid Media or Methylcellulose Solutions.** Approximately 20% of the total dermal volume in mammals consists of an entangled meshwork of types I and III collagen fibers (27, 28). *Bb* can bind directly to type I collagen (26) as well as other ECM constituents. To determine whether the motility of *Bb* in the dermis differs from that documented in liquid media and methylcellulose solutions, we used two-photon intravital confocal microscopy to track pathogen movement in the ears of mice that had been tick inoculated with Bb914, a virulent strain 297 isolate that constitutively expresses GFP (21). Spirochete movement was characterized by traveling-wave undulations of the cell body (Fig. 1*A*) as observed previously in liquid media, in methylcellulose solutions (19), and in the mouse dermis after i.v. injection (23). However, we also observed a major subpopulation of spirochetes that were actively motile but did not move through the dermis (Fig. 1*A*). These stationary, but motile, spirochetes occurred in two different states. Spirochetes in the first state, which we term *wriggling*, undulated as a traveling wave but otherwise remained fixed in place. In the other state, termed *lunging*, the spirochetes appeared to have one fixed end, while the remainder of the organism bent and relaxed as the organism apparently attempted to break free from its tether. These stationary states are likely due to adhesion between the bacteria and the ECM, as the spirochetes are still motile and are exerting forces on the ECM but are unable to translocate. Although we cannot directly probe whether the spirochetes in these states are actually physically bound to the matrix, it is quite probable that they are. In fact, the lunging state resembles the movement of *Bb* when it is tethered to a coverslip (19). For this reason, we classify this impedance as adhesion. The remainder of the bacteria, referred to as *translocating*, demonstrated a net displacement within the dermis. In general, these translocating spirochetes appeared similar to motile spirochetes in liquid media or methylcellulose; however, the fraction of translocating bacteria in the dermis was lower than that in liquid media or methylcellulose, where nearly all of the bacteria translocate. In addition, our observations suggest that spirochetes reverse their swimming direction less frequently in the dermis than in standard in vitro motility assays. Furthermore, we do not observe flexing motions, which are characteristic of spirochetes in liquid media (19). Therefore, at least three states of motility exist in the mouse dermis, two of which are not observed in liquid media or methycellulose solutions. The motility states were dynamic, as spirochetes in the dermis were observed to transition between them. For example, Fig. 1*A* shows a spirochete that switches from lunging to translocating (Movie S1). Another interesting feature of these heterogeneous motility states is that spirochetes in the different states were observed in close proximity to one another (Fig. 1*A*).

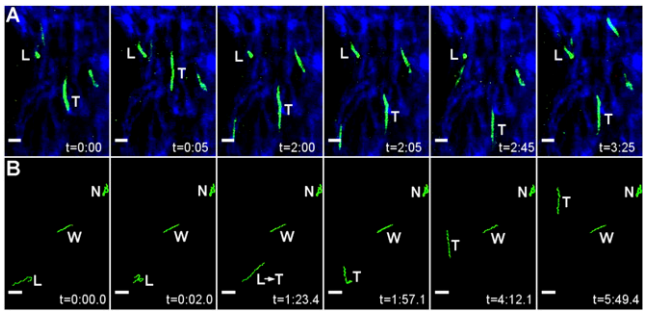

Fig. 1. The motility patterns of Lyme disease spirochetes (Bb914) in gelatin resemble those observed in mouse skin. (*A*) Time course of spirochetal (green) motility in the dermis of a tick-inoculated mouse (Movie S1). Lunging (L) and translocating (T) bacteria are shown. The dermal collagen fibers fluoresce blue due to second-harmonic generation. (*B*) Time course of *Bb* motility in 3% gelatin (Movie S2). All four motility states are shown: nonmotile (N), wriggling (W), lunging (L), and translocating (T). (Scale bars: 10 μm.)

***B. burgdorferi* Motility in Gelatin Resembles Motility in the Mouse Dermis.** To determine whether spirochetes within gelatin matrices show the same motility states as those observed in the dermis of the mouse, we examined the motility of Bb914 in 3% gelatin matrices using wide-field, epifluorescence, and confocal microscopy. In some experiments, microspheres were embedded into the matrix to guarantee that the spirochetes were within the gelatin (Movies S3 and S4). Spirochetes in the matrices exhibited all three types of motility seen in the dermis: wriggling, lunging, and translocating (Figs. 1*B* and 2*A*). In addition, high-speed acquisitions revealed a substantial fraction of spirochetes that were nonmotile, constituting a fourth behavior. This nonmotile state may also be present in the dermis but not seen due to the time interval between consecutive images in our intravital imaging (see *Adhesions to the Matrix Are Transient*).

Gelatin Concentration Affects Binding of Spirochetes to the Matrix. Having established that spirochete motility in our gelatin matrix system closely resembles that in tissues, we investigated the effect of gelatin concentration (2–5%) on the motility of *Bb*. We found that the fraction of bacteria in each motility state was strongly affected by the concentration of gelatin (Fig. 2*B*). Not surprisingly, increasing the concentration led to a larger population of nonmotile bacteria, which varied approximately linearly with gelatin concentration, ranging from 4.7 ± 2.4% in 2% gelatin to 35 ± 4% in 5% gelatin. The proportions of bacteria in the wriggling and lunging states decreased with increases in the gelatin volume fraction; however, the populations in the lunging state appeared to plateau at ~8% at the highest concentrations. The translocating population proved to be the most interesting state. As adhesion and confinement of the bacteria by the gelatin are more likely at higher gelatin concentrations, we had expected to find that the percentage of translocating bacteria would decrease with gelatin concentration. Instead, the fraction of translocating bacteria increased from 20.3 ± 0.5% in the 2% matrices to 35.5 ± 5.2% in the 3% matrices ($P = 0.042$); the populations then decreased to 24.5 ± 2.4% and 21.2 ± 4.2%, in the 4% and 5% matrices, respectively.

Swimming Speed of *B. burgdorferi* in Gelatin Matrices. Swimming speed in liquid media is determined by the wavelength, amplitude, and frequency of the undulating swimmer (2). Therefore, we measured speed and waveform of bacteria in the matrix system with a newly developed algorithm that parameterizes the centerline of the shape of bacteria in our time-lapse images (*SI Text S1* and Movie S5). From the parameterized shape, we computed the center of mass and the average orientation of the bacteria and then calculated swimming speed along the direction of the mean orientation. We found that translocating bacteria in the 3–5% gelatin matrices swam without slipping (i.e., the

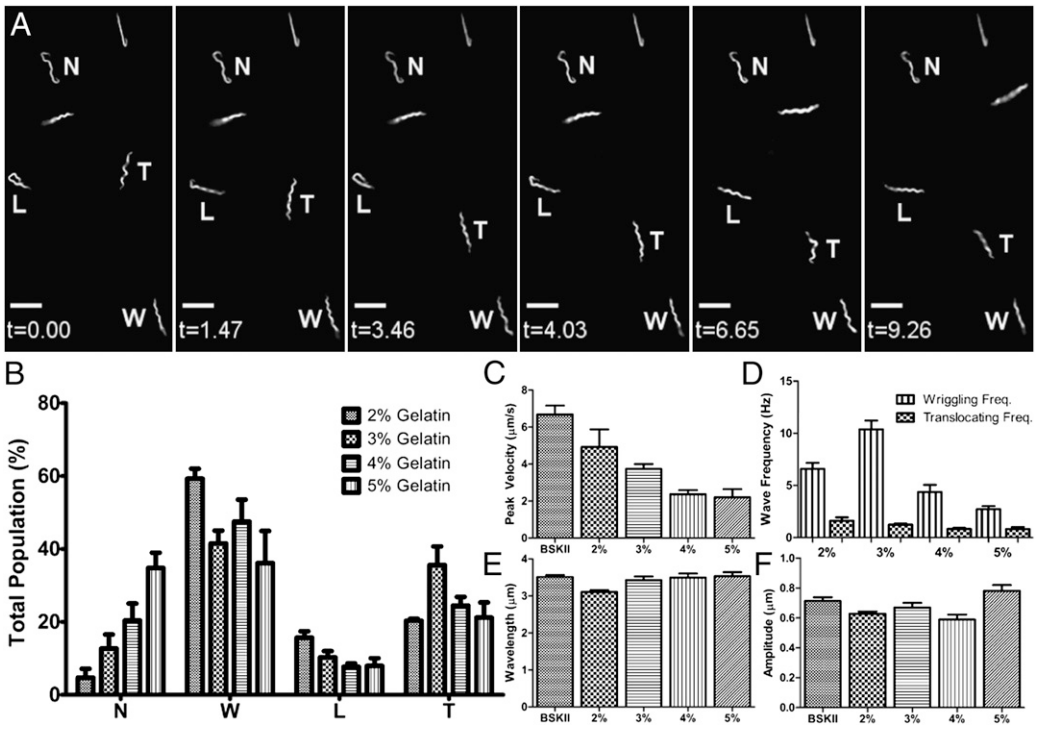

Fig. 2. (*A*) High-speed image acquisition reveals four distinguishable phases of spirochetal motility in gelatin (Movie S6): nonmotile (N), wriggling bacteria (W) that undulate without locomoting, lunging bacteria (L) that undulate and deform but maintain at least one fixed point along the cell length, and bacteria that translocate through the gelatin matrix (T). (Scale bar, 10 μm.) (*B*) The fraction of bacteria in each state depends on gelatin concentration. (*C*) The speed of translocating bacteria decreases with gelatin concentration and is always less than that in liquid medium. (*D*) The undulation frequency for translocating and wriggling bacteria as a function of gelatin concentration. The wriggling frequency always exceeds the translocating frequency and shows a peak in 3% gelatin solutions. (*E*) In all concentrations of gelatin and BSK, spirochete wavelengths were measured to be ~3.3 μm; (*F*) the amplitude is also independent of gelatin concentration.

swimming speed was equal to the wave speed), as has been observed for *Leptonema illini* in 1% methylcellulose solution (29) but is not predicted by any current theories for swimming in non-Newtonian fluids (9, 12, 13, 30). In the 2% matrices, translocating bacteria sometimes slip with respect to the matrix but still typically swim without slipping. The average swimming speeds of translocating bacteria in 2% and 3% gelatin matrices were 4.9 ± 1.0 μm/s and 3.7 ± 0.3 μm/s, respectively (Fig. 2*C*). Increasing the gelatin concentration further decreased the swimming speed (Fig. 2*C*). In comparison, the velocity of *Bb* in liquid medium [Barbour–Stoenner–Kelly II (BSK) medium] was 6.9 ± 0.7 μm/s, which is somewhat faster than previously reported for an avirulent 297 strain in salt buffer (19).

We also used the parameterized shape to compute the wavelength and amplitude of the flat-wave shape of *Bb*. We found that these cell shape parameters were unaffected by the concentration of gelatin, with an amplitude of 0.63 ± 0.03 μm and a wavelength of 3.31 ± 0.04 μm (combined mean ± SEM for all gelatin concentrations and BSK medium) (Fig. 2*D*). Our value of the amplitude is somewhat lower than that previously reported (19), which is likely due to segments of a spirochete's flat wave being out of the plane of focus. The wave frequency of the translocating bacteria is equal to the swimming speed divided by the wavelength and decreases from 1.6 ± 0.3·s^{-1} (2%) to 0.8 ± 0.2·s^{-1} (5%). We also measured the frequency of the wriggling bacteria. Interestingly, the wriggling frequency always exceeds the frequency of the translocators. The peak wriggling frequency was ~10 Hz in the 3% gelatin matrices (Fig. 2*E*), which is comparable to what has been measured in methylcellulose solutions (19). The wriggling frequency was slightly lower in 2% gelatin matrices (~7 Hz) and reduced further in 4% and 5% matrices (4 Hz and 3 Hz, respectively). The frequency in 3% gelatin was statistically significant compared with the frequencies in the other matrices ($P < 0.003$).

Microstructure of the Gelatin Matrices. From our high-speed imaging, it was not clear what determines the motility state of a given bacterium. One possibility is that the different states are determined by nonhomogeneity of the local environment. Another possibility is that adhesion to the matrix is stochastic, with the fraction of bacteria in a given motility state set by the kinetics of the binding and unbinding of adhesion proteins. Our time-lapse imaging favors the latter option, as we often see translocating spirochetes swimming very near wriggling or nonmotile bacteria. To investigate this question more fully, we used scanning electron microscopy (SEM) and transmission electron microscopy (TEM) to examine the microstructure of the gelatin matrices. We found that all concentrations of the gelatin matrices were homogeneous on length scales comparable to or larger than the diameter of *Bb* (~300 nm) (Figs. S1 and S2) and estimated from these images that the average pore size of the gelatin is <100 nm in the 2% matrices, ~50 nm in the 3% matrices, and slightly <50 nm in the 4–5% matrices. In addition, at all concentrations, the gelatin appeared to be in close contact with the organisms, and there was no noticeable difference in the gelatin structure as a function of distance from the surface of the bacterium (Fig. S2). These results suggest that the bacterium must push aside the gelatin filaments to enter and move through the matrix and that the gelatin is in close contact with the bacterial surface. Interestingly, the structure of the gelatin matrices closely resembles the basement membrane that lines the midgut of the tick (Figs. S2 and S5). In the dermis of a mouse ear, *Bb* were found to be tightly surrounded by collagen fibers (Figs. S2*H* and S5), which provides further evidence that the gelatin matrices are a good facsimile for studying *Bb* motility through the ECM and basement membrane.

Rheological Properties of the Gelatin Matrices. As demonstrated by the TEM images (Fig. S2), the gelatin matrices are extremely tight environments. For the bacteria to penetrate into the matrix, they must displace the gelatin to accommodate the diameter of the cell. We, therefore, characterized the mechanical properties of the gelatin matrices using shear rheology and estimated the Young's modulus of the gelatin matrices using a Poisson ratio of 0.4 (31). We found that the 2% matrices [Young's modulus of ~3 Pa (Fig. S3*A*)] were very soft and only nominally a gel, with a loss modulus that was comparable to the storage modulus for all frequencies that we explored. In the other matrices, the storage modulus was significantly larger than the loss modulus, and the

Young's modulus increased linearly from ~20 Pa (3% matrices) to ~300 Pa (5% matrices) (Fig. S2 *A* and *B*).

The gelatin must push in against the spirochete, requiring the organism to withstand this environmental pressure. If the pressure from the gelatin is at least comparable to the bacterial turgor pressure, then the diameter of the spirochete should depend on the gelatin concentration. Because no such change in diameter was observed (Fig. S4), we can put a lower bound on the turgor pressure in *Bb*, which must be at least 5 kPa to prevent the cell diameter from changing by >10%.

Adhesions to the Matrix Are Transient. Our intravital imaging in the dermis examined *Bb* motility over tens of minutes, whereas our high-speed imaging in gelatin spanned only tens of seconds. We, therefore, used confocal microscopy to examine spirochete motility in the gelatin matrices over longer time intervals. These movies revealed a much larger fraction of motile organisms than in the short time interval movies (Fig. 3*A* and Movie S7). In fact, movement of spirochetes in these movies more closely resembled our observations in the dermis, where the nonmotile fraction was not observed. Because the longer time interval movies show a significantly smaller percentage of nonmotile bacteria than the short time interval movies, adhesions between the bacteria and the matrix are likely transient. Indeed, as noted earlier and shown in Fig. 2*B*, we frequently observe bacteria that transition between different motility states. These results strongly suggest that differences between the motility states are dictated by the degree of adhesion between the bacterium and the matrix and that adhesions turn over on timescales of minutes.

Because the adhesions are transient, bacteria translocate for several seconds to minutes before becoming stuck. After a while, the bacteria break free and translocate again. If the spirochete swims off in a new direction after becoming stuck, then one would expect the behavior of the spirochete to be diffusive on long timescales; [i.e., the mean squared displacement (MSD) should scale linearly with time]. In all gelatin concentrations, we found that the MSD was subdiffusive on short timescales and transitioned to superdiffusive behavior on timescales of ~100 s (Fig. 3*B*). The average log-log slopes of the MSD data showed largely subdiffusive behavior (slopes <1); interestingly, the 5% matrices had the largest population of bacteria exhibiting superdiffusive behavior (Fig. 3*C*).

We were unable to observe diffusive behavior on longer timescales because translocating bacteria often traversed the entire field of view without becoming stuck. We could, nonetheless, use our confocal gelatin matrix data to determine whether our short-time interval observations were consistent with those obtained over longer time intervals. We determined that the number of bacteria that were tracked in a given field of view for at least a given length of time decays approximately exponentially (Fig. 3*D*). The time constant for this exponential decrease should be inversely proportional to the fraction of translocating bacteria, Φ_t, multiplied by the translocation velocity and also should be proportional to the size of the field of view (*SI Text S2*). A plot of the time constant as a function of $1/\Phi_t V$ (Fig. 3*D*, *Inset*) yields a straight line with a slope of 114 μm, which is approximately equal to half the size of our field of view. Therefore, the fractions of bacteria in the short time interval movies reflect an equilibrium in the transitions between the motility states.

Discussion

In this paper, we set out to develop an in vitro system to study *Bb* motility that would better approximate the natural host environments that *Bb* encounters (ticks and mice). Real time intravital imaging of host-adapted spirochetes in the dermis of mice revealed qualitative differences in motility in comparison with standard in vitro motility assays performed in liquid media containing salts or methylcellulose (19). In addition to a translocating population that swims via an undulating waveform, similar to spirochetes observed in vitro, we also found two other forms of motility, which we termed lunging and wriggling. These two forms of motility were characterized by at least one stationary point along the length of the bacterium. We then showed that in gelatin matrices these same motility states are observed; in addition, we also observe a fourth, nonmotile state. Whereas the nonmotile state appears similar to the stopped state observed in standard motility assays (15), the dependence of this state on gelatin concentration suggests that it arises from adhesion, as opposed to flagellar dynamics. It is likely that spirochetes in the nonmotile state are present in the dermis but are not observed due to the longer acquisition time of these images, as supported by the difference between our high-speed and confocal imaging in gelatin. Collectively, these findings argue that standard motility assays with either liquid media or methylcellulose solutions may not provide an accurate description of the motility of *Bb* in its natural environments. Finally, we quantified the biophysics of borrelial motility in gelatin. We found that the fraction of bacteria in each motility state is strongly dependent on the concentration of gelatin and that *Bb* can transition between translocating and lunging, between lunging and wriggling, and between wriggling and nonmotile states (Fig. 4*A*). Although we did not observe any other transitions, it could be that these occur infrequently. Our data suggest that these transitions are due to

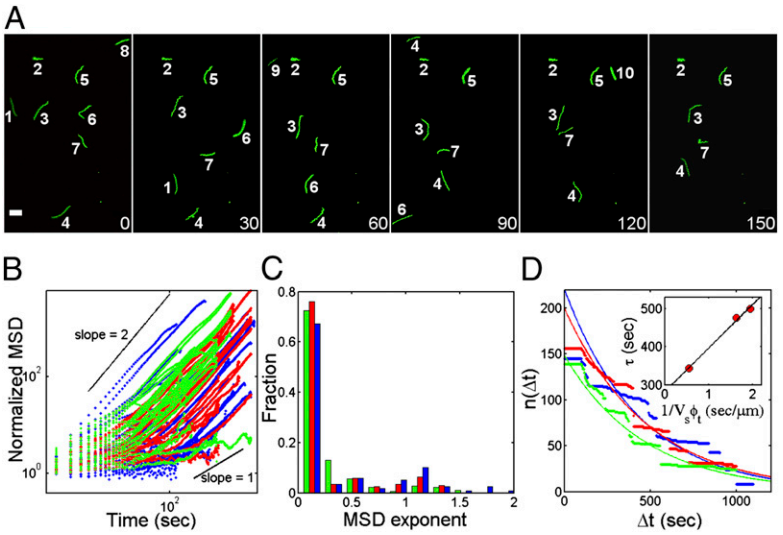

Fig. 3. (*A*) Time-lapse images of *Bb* in a 3% gelatin matrix show that adhesions to the matrix are transient (Movie S7). Individual spirochetes are numbered. Most are translocating (spirochetes 1, 3, 4, 6–10). Nonmotile (2) and wriggling (5) spirochetes also are shown. (Scale bar, 10 μm.) (*B*) Characteristic MSD vs. time plots for the 3–5% gelatin matrices. In all concentrations, the motility over short time intervals is subdiffusive, with a transition to superdiffusive behavior (slope between 1 and 2) that occurs at ~100 s. (*C*) Histogram of the slopes of the MSD for the different gelatin concentrations. The 5% matrices show the greatest persistence of motion (i.e., the largest fraction with slopes >1). Black lines show slopes of 1 and 2. (*D*) The number of bacteria tracked for at least a time Δt decays approximately exponentially. (*Inset*) Decay time as a function of $1/\Phi_t V$, which is linear with slope of 114 μm. (*B–D*) Plot coloring shows 3% (green), 4% (red), and 5% (blue) gelatin.

transient adhesions between the bacterium and the gelatin. One of the most interesting features of the population data is the peak in the translocating population in the 3% gelatin matrices (Fig. 2*B*). There is also a corresponding peak in the wriggling frequency in 3% matrices (Fig. 2*E*); however, the swimming speed and the wave frequency of the translocators decrease monotonically (Fig. 2*D*).

Adhesion between *Bb* and host tissues is believed to play an important role in the parasitic strategy of the bacterium and has been studied extensively (24). Typical adherence assays determine the number of spirochetes that remain on a surface after washing (see, for example ref. 26), which quantifies instantaneous adhesion. Our results suggest that adhesion in the dermis and gelatin is a dynamic process in which the bacteria can bind and unbind from the matrix. From our population data, we can characterize the effect of gelatin concentration on the adhesions between the bacteria and the gelatin (Fig. 4*B*) and can also estimate the time constants for these reactions. Our results suggest that the rate of binding to the matrix is affected by the concentration of adhesins, as the nonmotile state increases with gelatin concentration. The unbinding rate, however, is not likely affected by the concentration, because our MSD data show a change in slope at ~100 s at all gelatin concentrations, suggesting that the binding and unbinding rates are on the order of 10 ms. We presume that the translocating population possesses no fixed adhesions to the matrix, whereas the nonmotile population possesses the largest number of adhesions. If forces between the spirochete and the gelatin affect the unbinding of adhesion molecules, then the equilibrium rate constants K_{wl} and K_{lt} divided by the gelatin concentration should decrease monotonically with the square of the effective viscosity of the matrix, η, times the undulation frequency, f (*SI Text S3*). Our data agrees well with this prediction (Fig. 4*C*). Therefore, the binding rate is likely proportional to the gelatin concentration and the off rate increases with applied force from the motile spirochete.

It is often stated that spirochetes swim faster in gel-like environments than in liquid media, and this property is believed to be important for the dissemination of the bacteria through their hosts (16, 19, 32, 33). For example, *Bb* and *L. illini* show marked increases in speed in 1% methylcellulose solutions (29, 33). Our results, though, show a decrease in swimming speed with gelatin concentration that is caused by a substantial decrease in the undulation frequency. However, although *Bb* swims slower in gelatin, it swims without slipping. Therefore, the ratio of the swimming speed to the wave speed is larger by approximately a factor of 10 over that measured in liquid media (*SI Text S4*). Recent computational modeling has shown that viscoelasticity can enhance swimming speed for undulating bodies with a pronounced increase in amplitude at the tail (30), and experiments with rotating helices have shown a similar effect (34). Both of these cases, however, show only modest speed enhancement, and in neither case is swimming without slipping observed.

We did not expect that the wriggling frequency would always be substantially larger than the wave frequency of the translocating bacteria. However, wriggling bacteria dissipate energy only by undulating, whereas translocators also dissipate energy by moving through the matrix. Because the total power dissipated must be equal to the power input by the flagellar motors, the frequency of translocators should be lower than that of wrigglers. At low rotational speed, the torque from the flagellar motor is approximately constant (35). The power input is equal to the torque times the frequency. The power dissipated comes from two sources, rotating the flagellum in the periplasmic space and moving the bacterium through the environment. Using a simple model for swimming through a gel, we can estimate the total power dissipated (*SI Text S5*). The effective viscosity of the gelatin matrix should then be linearly proportional to the inverse of the undulation frequency, as $1/f = \alpha\beta\eta + c$, where β and c are constants and $\alpha = 1$ for wriggling and 7/2 for translocating (*SI Text S5*). This theoretical result predicts that the undulation frequency is largely independent of the matrix elasticity. We tested this prediction using our rheology measurements to define η (Fig. S2*B*) and found good agreement between the predicted behavior and our experimental measurements (Fig. 4*D*). In methylcellulose solutions, *Bb* swims without slipping, but the undulation frequency is seemingly unaffected. It is not clear why this behavior occurs, but it could be that these solutions are viscoelastic fluids, not gels, or that the concentrations that are used (<1%) are low enough that the bacterium is not always in direct contact with the polymer.

Dissemination of *Bb* within its arthropod vector and mammalian hosts, as well as transitioning between them, relies upon the spirochete's ability to move through dense tissues. It is interesting to speculate as to why the motility states that we observe in the dermis and in gelatin may be important during the enzootic cycle. The tick midgut seems to be a hospitable environment for *Bb*, as the spirochetes are found in high abundance at this site (21, 36, 37). However, during the blood meal, some spirochetes must leave the tick and transition to the mammalian host for the species to survive (38). Egress from the tick midgut is likely a difficult process, accomplished only by an astonishingly few spirochetes (21, 39). Traversal of the midgut into the hemolymph involves adhesion and wiggling given the tight spaces the spirochete has to maneuver through [i.e., epithelial cell junctions and the basement membrane (Figs. S2 and S5)]. Although our experiments do not directly probe the mechanism by which spirochetes penetrate dense matrices, it is clear that the undulatory swimming of *Bb* enables these bacteria to migrate through fairly dense polymer networks; however, motility is inhibited in dense matrices, which explains why so few organisms are able to escape the midgut (21).

Once in the mammal, *Bb* need to disseminate through the host to evade the host immune response, enter the bloodstream, find hospitable tissue in which to replicate efficiently, and return to the dermis to infect new ticks (38). The translocaters, therefore, play a vital role in spirochete dissemination throughout the mammal. Swimming solely in one direction, though, is not a good means for spreading within an environment. Rather, many

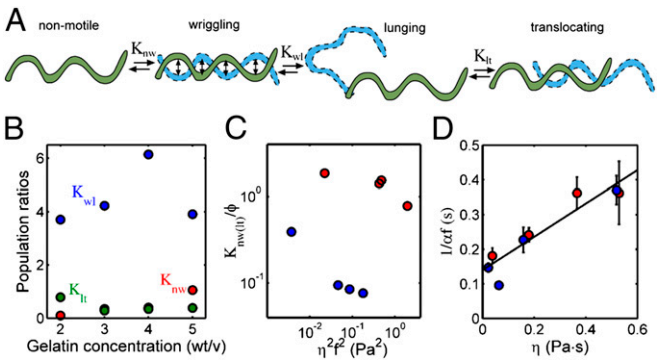

Fig. 4. A simple kinetic model determines the effective rate constants for binding and unbinding to the matrix as a function of gelatin concentration. Transitions occur between the nonmotile and wriggling states, between the wriggling and lunging states, and between the lunging and translocating states. If these transitions are in equilibrium, then the equilibrium rate constants are equal to the ratios of the fraction of bacteria in the states; (e.g., the equilibrium constant for the transition between nonmotile and wriggling, K_{nw}, is equal to the ratio of the fractions of nonmotile bacteria to lunging bacteria). (*B*) The equilibrium constants as a function of gelatin concentration. The transition from wriggling to nonmotile, K_{nw}, increases approximately linearly with gelatin concentration. (*C*) K_{wl} and K_{lt} are also proportional to gelatin concentration (ϕ) and also decrease with the force from the bacterium (which is proportional to the square of the effective viscosity η times the undulation frequency, f). (*D*) The inverse of the frequency of wrigglers (red) and translocators is proportional to the viscosity. The parameter $\alpha = 1$ for wrigglers and 7/2 for translocators (*SI Text S4*). The black line shows the best linear fit to the data.

microorganisms use random walks, such as the run-and-tumble behavior of *Escherichia coli* (35). In vitro experiments of *Bb* motility display two modes of swimming, runs and flexes, which were suggested to be analogs of runs and tumbles in *E. coli* (15). However, we did not observe flexing in the dermis or gelatin. We, therefore, suggest that lunging may be the equivalent of tumbling. Translocating bacteria move along relatively straight paths. When the spirochetes adhere to the matrix, they lunge by compressing along their longitudinal axis and then uncompressing in a new direction. Because the adhesions are transient, some lungers break free and swim off in a new direction. The lunging state then serves to periodically reorient bacteria, much like a tumble.

What roles might the wriggling and nonmotile states serve? To complete the enzootic cycle, spirochetes must strategically position themselves in the dermis to be acquired by another tick. The stationary states (nonmotile and wriggling) may be a mechanism for keeping higher burdens of spirochetes in collagen-rich tissues like the skin. In addition, these stationary states might be part of the spirochete's strategy for immune evasion. Stationary bacteria would be more susceptible to internalization by much slower moving resident and recruited phagocytes, effectively acting as decoys that would facilitate dissemination of translocating bacteria. However, whatever the functional role is of these different motility states, our data show a striking example of spirochete diversity. Transient adhesions act to subdivide the bacterial population into multiple motility states, even in fairly uniform tissue-like environments. This diversity may allow *Bb* to exploit changing environments and host-mediated environmental responses and is likely to be important in the enzootic cycle and the progression of disease.

Materials and Methods

Here we give a brief description of the methods. See *SI Text S1* for a complete description.

All experiments were done using Bb914 (26), which were grown to late log-phase in BSK II medium supplemented with 6% normal rabbit serum (Pel-Freeze Biologicals).

Mouse experiments used C57BL/6 mice (4–6 wk old), purchased from The Jackson Laboratory, and were conducted following the National Institutes of Health guidelines for housing and care of laboratory animals and were performed under animal protocols approved by the Yale University Institutional Animal Care and Use Committee. Infection was introduced into mice using laboratory-reared *I. scapularis* nymphal ticks infected as larvae with Bb914, as described in refs. 21 and 40. Mice were imaged 98 d after infection, using an Olympus BX61WI fluorescence microscope with a 20×, 0.95 NA water immersion Olympus objective and a dedicated single-beam LaVision TriM laser scanning system (LaVision Biotec) that was controlled by Imspector software.

Gelatin stocks were prepared by dissolving Type-A gelatin powder in sterile PBS, as previously described (21). A total of 5×10^7 spirochetes in BSK II were introduced onto the top of each gelatin matrix and incubated in the dark for 1 h. High-speed videos were captured on a BX41 microscope (Olympus) equipped with a Retiga Exi Fast CCD camera (QImaging) with StreamPix 3 software (Norpix). Long-term videos were captured on an LSM 510 Meta (Zeiss) with the aperture fully open.

ACKNOWLEDGMENTS. The authors thank E. Dufresne, R. Boltyanskiy, and C. Osuji for performing the rheology experiments and N. Charon for useful discussions. This research was supported by National Institutes of Health Grant R01GM072004 (to C.W.W.); National Institutes of Health Grant R01AI085798 and the Jockers Award (to L.K.B.); National Institutes of Health Grants R01AI029735 and 3R01AI029735-20S1 (to J.D.R. and M.J.C.); and National Institutes of Health Grants R01AI26756 (to J.D.R.), R03AI085248 (to M.J.C.), and U54AI057159 (to S.M.D.-E.).

1. Wolgemuth CW (2011) Biomechanics of cell motility. *Comprehensive Biomechanics*, ed Wirtz D (Elsevier, Amsterdam), Vol 7, in press.
2. Taylor GI (1951) Analysis of the swimming of microscopic organisms. *Proc R Soc Lond A Math Phys Sci* 209:447–461.
3. Taylor GI (1952) The action of waving cylindrical tails in propelling microorganisms. *Proc R Soc Lond A Math Phys Sci* 211:225–239.
4. Purcell EM (1977) Life at low Reynolds number. *Am J Phys* 45:3–11.
5. Croll NA (1970) *The Behavior of Nematodes: Their Activity, Senses and Responses* (Edward Arnold, London).
6. Fang-Yen C, et al. (2010) Biomechanical analysis of gait adaptation in the nematode *Caenorhabditis elegans*. *Proc Natl Acad Sci USA* 107:20323–20328.
7. Shen XN, Arratia PE (2011) Undulatory swimming in viscoelastic fluids. *Phys Rev Lett* 106:208101.
8. Suarez SS, Dai XB (1992) Hyperactivation enhances mouse sperm capacity for penetrating viscoelastic media. *Biol Reprod* 46:686–691.
9. Fu HC, Powers TR, Wolgemuth CW (2007) Theory of swimming filaments in viscoelastic media. *Phys Rev Lett* 99:258101.
10. Fu HC, Wolgemuth CW, Powers TR (2008) Beating patterns of filaments in viscoelastic fluids. *Phys Rev E Stat Nonlin Soft Matter Phys* 78:041913.
11. Fu H, Wolgemuth CW, Powers TR (2009) Swimming speeds of filaments in nonlinearly viscoelastic fluids. *Phys Fluids* 21:033102.
12. Fu HC, Shenoy VB, Powers TR (2011) Low Reynolds-number swimming in gels. *Eur Phys Lett* 91:24002.
13. Lauga E (2007) Propulsion in a viscoelastic fluid. *Phys Fluids* 19:083104.
14. Fulford GR, Katz DF, Powell RL (1998) Swimming of spermatozoa in a linear viscoelastic fluid. *Biorheology* 35:295–309.
15. Goldstein SF, et al. (2010) The chic motility and chemotaxis of Borrelia burgdorferi. *Borrelia: Molecular Biology, Host Interaction and Pathogenesis*, eds Samuels DS, Radolf JD (Caister Academic, Norfolk, UK), pp 167–188.
16. Charon NW, Goldstein SF (2002) Genetics of motility and chemotaxis of a fascinating group of bacteria: The spirochetes. *Annu Rev Genet* 36:47–73.
17. Wolgemuth CW, Charon NW, Goldstein SF, Goldstein RE (2006) The flagellar cytoskeleton of the spirochetes. *J Mol Microbiol Biotechnol* 11:221–227.
18. Dombrowski C, et al. (2009) The elastic basis for the shape of Borrelia burgdorferi. *Biophys J* 96:4409–4417.
19. Goldstein SF, Charon NW, Kreiling JA (1994) *Borrelia burgdorferi* swims with a planar waveform similar to that of eukaryotic flagella. *Proc Natl Acad Sci USA* 91:3433–3437.
20. Haake DA (2010) Introduction. *Borrelia: Molecular Biology, Host Interaction and Pathogenesis*, eds Samuels DS, Radolf JD (Caister Academic, Norfolk, UK), pp 1–6.
21. Dunham-Ems SM, et al. (2009) Live imaging reveals a biphasic mode of dissemination of Borrelia burgdorferi within ticks. *J Clin Invest* 119:3652–3665.
22. Pal U, Fikrig E (2010) Tick interactions. *Borrelia: Molecular Biology, Host Interaction and Pathogenesis*, eds Samuels DS, Radolf JD (Caister Academic, Norfolk, UK), pp 279–298.
23. Moriarty TJ, et al. (2008) Real-time high resolution 3D imaging of the lyme disease spirochete adhering to and escaping from the vasculature of a living host. *PLoS Pathog* 4:e1000090.
24. Cabello FC, Godfrey HP, Newman SA (2007) Hidden in plain sight: Borrelia burgdorferi and the extracellular matrix. *Trends Microbiol* 15:350–354.
25. Leitinger B, Hohenester E (2007) Mammalian collagen receptors. *Matrix Biol* 26: 146–155.
26. Zambrano MC, Beklemisheva AA, Bryksin AV, Newman SA, Cabello FC (2004) Borrelia burgdorferi binds to, invades, and colonizes native type I collagen lattices. *Infect Immun* 72:3138–3146.
27. Yasui T, Tohno Y, Araki T (2004) Characterization of collagen orientation in human dermis by two-dimensional second-harmonic-generation polarimetry. *J Biomed Opt* 9:259–264.
28. Saidi IS, Jacques SL, Tittel FK (1995) Mie and Rayleigh modeling of visible-light scattering in neonatal skin. *Appl Opt* 34:7410–7418.
29. Goldstein SF, Charon NW (1990) Multiple-exposure photographic analysis of a motile spirochete. *Proc Natl Acad Sci USA* 87:4895–4899.
30. Teran J, Fauci L, Shelley M (2010) Viscoelastic fluid response can increase the speed and efficiency of a free swimmer. *Phys Rev Lett* 104:038101.
31. Markidou A, Shih WY, Shih W-H (2005) Soft-materials elastic and shear moduli measurements using piezoelectric cantilevers. *Rev Sci Instrum* 76:064302.
32. Berg HC, Turner L (1979) Movement of microorganisms in viscous environments. *Nature* 278:349–351.
33. Kimsey RB, Spielman A (1990) Motility of Lyme disease spirochetes in fluids as viscous as the extracellular matrix. *J Infect Dis* 162:1205–1208.
34. Liu B, Powers TR, Breuer KS (2011) Force-free swimming of a model helical flagellum in viscoelastic fluids. *Proc Natl Acad Sci USA* 108:19516–19520.
35. Berg HC (2003) The rotary motor of bacterial flagella. *Annu Rev Biochem* 72:19–54.
36. Levin M, Papero M, Fish D (1997) Feeding density influences acquisition of Borrelia burgdorferi in larval Ixodes scapularis (Acari: Ixodidae). *J Med Entomol* 34:569–572.
37. Piesman J, Oliver JR, Sinsky RJ (1990) Growth kinetics of the Lyme disease spirochete (*Borrelia burgdorferi*) in vector ticks (*Ixodes dammini*). *Am J Trop Med Hyg* 42: 352–357.
38. Tilly K, Rosa PA, Stewart PE (2008) Biology of infection with *Borrelia burgdorferi*. *Infect Dis Clin North Am* 22:217–234, v.
39. Coleman JL, et al. (1997) Plasminogen is required for efficient dissemination of B. burgdorferi in ticks and for enhancement of spirochetemia in mice. *Cell* 89:1111–1119.
40. Bockenstedt LK, et al. (1997) *Borrelia burgdorferi* strain-specific Osp C-mediated immunity in mice. *Infect Immun* 65:4661–4667.

Supporting Information

Harman et al. 10.1073/pnas.1114362109

SI Text S1. Methods

Bacterial Strains and Media. Bb914, a derivative of *Borrelia burgdorferi* strain 297 that constitutively expresses *gfp* driven by the *flaB* promoter (1), was used in all experiments. Frozen aliquots of low-passage spirochetes were temperature shifted to 37 °C and grown to late log-phase in Barbour–Stoenner–Kelley II (BSK) medium supplemented with 6% normal rabbit serum (Pel-Freeze Biologicals). Spirochetes were enumerated using a Petroff–Hausser counting chamber before each experiment and harvested at a culture density near 1×10^8 spirochetes per milliliter.

Mice. C57BL/6 mice (4–6 wk old), purchased from The Jackson Laboratory, were housed in filter frame cages and administered food and water ad libitum. All mouse experiments were conducted following the National Institutes of Health guidelines for housing and care of laboratory animals and were performed under animal protocols approved by the Yale University Institutional Animal Care and Use Committee.

Tick Infestation of Mice. Infection was introduced into mice using laboratory-reared *Ixodes scapularis* nymphal ticks infected as larvae with Bb914, as described in refs. 2 and 3. Briefly, mice were anesthetized with 100 mg/kg ketamine (Butler Schein) and 10 mg/mg xylazine (Butler Schein) to immobilize them before placement of nymphs in the head region (five nymphs per mouse). Ticks were allowed to feed to repletion and collected after natural detachment into a water bath. Infection was confirmed at 14 d by seroconversion as assessed by immunoblot.

Intravital Imaging. Mice were imaged 98 d after Bb914 infection was introduced by tick feeding. Mice were anesthetized by i.p. injection with a mixture of 100 mg/kg ketamine and 10 mg/kg xylazine before shaving and denuding the ear skin with Nair (Armkel). The anesthetized mouse was then immobilized on a custom-designed stereotactic restraint platform. A plane of deep anesthesia was maintained using a mixture of isofluorane gas and oxygen delivered via a nosecone. Imaging of spirochetes in ear skin was conducted in real time, using an Olympus BX61WI fluorescence microscope with a 20×, 0.95 NA water immersion Olympus objective and a dedicated single-beam LaVision TriM laser scanning system (LaVision Biotec) that was controlled by Imspector software. The microscope was outfitted with a Chameleon Vision II Ti:Sapphire laser (Coherent) with pulse precompensation. Image stacks of five optical sections with 3 μm *z* spacing were acquired every 5 s for 10 min with the laser tuned to a wavelength of 940 nm. Each *xy* plane spanned 300 μm in each dimension with an *xy* resolution of 0.59 μm per pixel. Volocity software (Improvision) was used to create QuickTime formatted movies of image sequences, which were displaced as 2D maximum intensity projections.

Gelatin Preparation. Gelatin stocks were prepared by dissolving 2–5% (wt/vol) of Type-A gelatin powder from porcine skin (Sigma) in sterile PBS while stirring at a steady temperature of 56 °C, as previously described (3). The gelatin stocks were stored at 4 °C and used to prepare the matrix slides at least 1 d, but no longer than 1 wk, before performing the imaging experiments. The solidified gelatin was allowed to stand at room temperature (RT) before being warmed on low heat. 350 μL aliquots of liquefied gelatin were added to each well of a chamber slide (BD Falcon), while cautiously avoiding introduction of bubbles. The slides were wrapped in a humidified chamber and placed at 4 °C on a level surface to set.

A few hours before imaging, the slides were equilibrated to RT. A total of 5×10^7 spirochetes in BSK were introduced onto the top of each gelatin matrix and incubated in the dark at RT for 1 h. The supernatant was removed and each well was washed twice with 400 μL of sterile PBS. A sterile surgical blade (Bard-Parker) was run twice around the perimeter of each gelatin matrix, the plastic chambers were removed, a minimal volume of PBS was added, and an extended coverslip (Fisher Scientific) then was carefully applied.

Real-Time Imaging of Spirochete Motility in Gelatin Matrices. To determine the modes of spirochete motility, high-speed (40 frames/s) videos were captured on a BX41 microscope (Olympus) equipped with a Retiga Exi Fast CCD camera (QImaging) with StreamPix 3 software (Norpix). For long-term videos (~1 frame/s), spirochete motility was captured on an LSM 510 Meta (Zeiss) with the aperture fully open.

To confirm that bacteria were inside the gelatin matrices, in some experiments, 500-nm fluorescent microspheres (Invitrogen) were embedded in the gelatin matrices by mixing the spheres in the liquid gelatin before solidification. By comparing the magnitude of the thermal fluctuations of the spheres with what is observed in BSK media (which is a liquid medium), we could easily determine that the bacteria were inside the matrices (Movies S3 and S4).

Transmission Electron Microscopy. To determine the pore size of the gelatin matrices, fragments of 2–5% gelatin were fixed in 0.1 M sodium cacodylate (CAC) buffer containing 4% paraformaldehyde and 2.5% glutaraldehyde overnight at 4 °C. The gelatin was then postfixed in 0.1 M CAC buffer containing 1% OsO_4, and 0.8% potassium ferricyanide. The samples were then washed in water, stained in 1% uranyl acetate, and dehydrated in ascending ethanol solutions. The gelatin was then infiltrated and embedded in PolyBed 812. Thin sections (70 nm) were cut on an ultramicrotome (Leica), collected on formvar-coated slot grids and/or 300 Cu mesh grids, and stained in 2.5% uranyl acetate and lead citrate. The stained sections were viewed on a Hitachi H-7650 transmission electron microscope. Images were acquired using an AMT camera and Image Capture Engine v6.01 software (Advanced Microscopy Techniques). To determine the morphology of spirochetes within the gelatin matrices, 1×10^{10} spirochetes were incubated on 150 μL solidified gelatin for a minimum of 2 h. The gelatin/spirochete mixture was fixed overnight at 4 °C in 0.1 M CAC buffer containing 4% paraformaldehyde and 2.5% glutaraldehyde, as above. The samples were then processed as described for the gelatin alone.

Determination of the Motility Modes. Manual review of the high-speed real-time images was performed to categorize the spirochetes into one of four modes of motility: (*i*) Spirochetes were ranked as translocating (net translational movement) if the entire spirochete made net progress through the matrix. (*ii*) Spirochetes were considered to be lunging if one region, usually an end of the bacterium, remained fixed while the rest of the spirochete made large displacements within the gelatin. The cell body of a lunging bacterium typically bends and straightens as a function of time. (*iv*) Wriggling spirochetes undulated without making any appreciable displacements in the matrix. (*v*) Spirochetes were deemed nonmotile if there was no movement of

the cell body during the course of the movie. Over 2,500 organisms were categorized from three separate experiments for each gelatin percentage. The mode of motility was observed over the entire span of the video (10 s). Spirochetes were excluded from the analysis if their motility could not be accurately and consistently categorized.

Although it is easy to distinguish between the motility modes by visual inspection of the spirochete motility, we also sought to develop a quantitative metric for determining the motility modes. We tracked the end positions and the center of mass position of spirochetes that were tracked for at least 20 frames during the course of each time series (see below for a description of the algorithm that was used to track the bacterial centerlines). Spirochetes are classified as nonmotile or wriggling if the displacement of the center of mass moved <12 pixels (~2.2 μm) in 2% gelatin, <10 pixels (1.8 μm) in 3% and 4% matrices, or <8 pixels (1.4 μm) in 5% matrices over the course of the time series. For bacteria that made larger displacements, we computed the correlation of the displacements of the ends. If the ends of the bacterium had positions defined by $\mathbf{x}_1$ and $\mathbf{x}_2$, then we compute the correlation

$$C = \frac{\sum_i (\mathbf{x}_1(t_i) - \bar{\mathbf{x}}_1)\cdot(\mathbf{x}_2(t_i) - \bar{\mathbf{x}}_2)}{\sum_j \sqrt{(\mathbf{x}_1(t_j) - \bar{\mathbf{x}}_1)^2} \sum_j \sqrt{(\mathbf{x}_2(t_j) - \bar{\mathbf{x}}_2)^2}}, \qquad [S1]$$

where a bar over the variable denotes the average value. If the absolute value of C is >0.3, then the motion of the ends is well correlated, and the bacterium is classified as a translocator; otherwise the bacterium is classified as a lunger. In this way we quantify and automate the classification of the bacteria into stationary (nonmotile or wriggling), translocating, or lunging modes. This quantitative metric agrees with our visual classification to ~90%. We have not tested any algorithms to distinguish between the two stationary modes.

Image Analysis. The frequency of wave propagation in the "wriggling" population was assessed in each gelatin concentration using ImageJ software (National Institutes of Health). The time required for the peak of the waveform to cycle through a single location was assessed. Periods of rest (i.e., when the waveform was not propagating) were excluded from the measurements. Over 260 wave periods were measured from 25 organisms. We determined that most of the translocating bacteria swam without slipping. Therefore, the frequency of the translocating bacteria could be determined by dividing the velocity by the wavelength. For this analysis, we analyzed specific frames over which the translocating bacteria were making net progress through the matrix. Velocity, wavelength, and amplitude of the spirochetes were measured using a MATLAB algorithm that we developed. The algorithm computes the backbone shape and location of the center of mass of bacteria from fluorescent images by combining a thresholded image and a moving least-squares algorithm (4). The wavelength and the amplitude of the flat-wave shape were analyzed using Fourier analysis, unless the bacteria were deformed (i.e., lunging spirochetes). A quartic function was used to correct the shape of deformed bacteria. Fourier analysis of the shape yielded the wavelength and amplitude of the undeformed cell shape. Velocities were calculated by subtracting the center of mass position of the cell at one time point from the position at the preceding time point. The x component of the velocity was calculated as the difference between the x coordinate of the center of mass at time $t + dt$ and the x coordinate at time t/dt, with a similar calculation for the y component of the velocity.

To analyze the speed of the bacteria, we computed the component of the velocity of the bacterium in the direction of the average orientation of the cell. To reduce noise in these calculations, we applied a 40-point running average of the computed velocities. As many bacteria reversed direction during the course of a time series, we fitted the velocity profiles to a sinusoidal wave. The maximum velocity of the bacterium is then the maximum amplitude of the sinusoid.

The pore size of the gelatin matrices was estimated using the power spectrum of the Fourier transforms of the EM images. Two peaks were observed, one at short wavelengths and the other at an intermediate wavelength. We took this secondary peak to represent the mean pore size. The numbers we found were in good agreement with manual measurements done using ImageJ.

To assess the influence of gelatin concentration on spirochete shape, the inner membrane diameter was measured in cross-sectional TEM images using ImageJ. Three different diameter measurements were averaged for each spirochete in each gelatin concentration and in BSK media.

Rheological Measurements of the Gelatin. Mechanical properties were quantified using cone and plate geometry in a shear rheometer (ARES-LS1). We used 50-mm diameter tools with a 2° cone. Some measurements were repeated using a 1° cone to verify results. Gelatin solutions at ~56 °C were injected into the rheometer tool, temperature controlled at 4 °C. The elastic modulus was monitored over time to ensure that the gel had formed and its properties were not significantly changing over time. An amplitude sweep was performed to determine the range of linear elastic response of the gel. Finally, the elastic and viscous moduli were measured as a function of frequency.

Statistical Analysis. To determine whether differences in the populations, amplitudes, wavelengths, speeds, or frequencies were statistically significant, we analyzed our data using Student's t tests to compare datasets to each other and determine the probability that the two datasets represented a single distribution. P values <0.05 were considered to be statistically significant. We used the MATLAB routine ttest2 to compute the P values.

SI Text S2. Calculation of the Time Constant for the Length of Time That Bacteria Are Tracked in the Confocal Images

We defined the number of bacteria in the field of view as N and the characteristic size of the field of view as L. The total number of bacteria in the field of view was further subdivided according to the time at which the bacteria entered the field of view. That is, we defined the density of bacteria at time t that entered the field of view at time $t - \Delta$, $n(t, \Delta)$. The total number of bacteria in the field of view is then given by

$$N(t) = \int_{-\infty}^{0} n(t, \Delta) d\Delta. \qquad [S2]$$

We assumed that we could track bacteria as long as they were in the field of view and that bacteria leave or enter the field of view only if they are in the translocating fraction, denoted by Φ_t, which swims with average speed V. The time rate of change of n is then

$$\frac{\partial n}{\partial t} + \frac{\partial n}{\partial \Delta} = -\frac{V}{L}\Phi_t n + \text{Area} \times \text{Flux} \times \delta(\Delta), \qquad [S3]$$

where Area is the surface area of the confocal volume and Flux is the number of translocating bacteria that enter the volume as a function of time. Bacteria that swam into the field of view at time t have $\Delta = 0$, which is prescribed by the Dirac delta function, $\delta(\Delta)$. We assumed that our confocal images are in dynamic

equilibrium; (i.e., we look for the steady-state solution to Eq. **S2**). Therefore,

$$n(\Delta) \propto e^{\frac{-V\Phi_t}{L}\Delta}. \quad \text{[S4]}$$

If we measure the fraction of bacteria that are tracked for at least a time Δ, we expect this fraction to decay exponentially with time constant $L/V\Phi_t$. Because we measure V and Φ_t using high-speed microscopy, and we measure the time constant from longer time imaging, this measurement provides insight into whether the behaviors of the bacteria over these two different timescales are consistent with one another.

SI Text S3. Theoretical Predictions for the Effect of Gelatin Concentration and Applied Force on the Equilibrium Rate Constants

If the transitions between the motility states represent a dynamic equilibrium, then we expect that we can describe the populations in each state as being determined by the steady state of a reaction system given by

$$\begin{aligned} N &\underset{k_2}{\overset{k_1}{\rightleftharpoons}} W \\ W &\underset{k_4}{\overset{k_3}{\rightleftharpoons}} L \\ L &\underset{k_6}{\overset{k_5}{\rightleftharpoons}} T, \end{aligned} \quad \text{[S5]}$$

where N, W, L, and T represent the fraction of bacteria in the nonmotile, wriggling, lunging, and translocating populations, respectively. Here, k_1, k_3, and k_5 are unbinding rates and k_2, k_4, and k_6 are binding rates. The equilibrium constants are then

$$\begin{aligned} K_{nw} &= \frac{N}{W} = \frac{k_2}{k_1} \\ K_{wl} &= \frac{W}{L} = \frac{k_4}{k_3} \\ K_{lt} &= \frac{L}{T} = \frac{k_6}{k_5}. \end{aligned} \quad \text{[S6]}$$

We expect that the binding rates should be proportional to the concentration of the gelatin, ϕ. In addition, when the bacteria are bound to the matrix and actively motile, they exert force on the matrix. Thermodynamics suggest that the off rate should be proportional to the exponential of the energy in the adhesion bond divided by Boltzmann's constant times the temperature, as in the Bell model (5). If the adhesion molecules can be modeled as Hookean springs, then the elastic energy in the bond is $1/2\ \kappa x^2$, where κ is the spring constant. The force that the spirochete exerts against the matrix comes from the thrust force, which should be proportional to the viscosity, η, times the undulation frequency, ω. Therefore, we expect that the elastic energy in the adhesion is proportional to the square of the viscosity times the undulation frequency. This force should affect the off rate, but should not influence the on rate. Therefore, we expect that

$$\begin{aligned} K_{nw} &= a_1\phi \\ K_{wl} &= a_2\phi e^{-b_2\eta^2\omega^2} \\ K_{lt} &= a_3\phi e^{-b_3\eta^2\omega^2}, \end{aligned} \quad \text{[S7]}$$

where the as and bs are constants. K_{nw} should not depend on the frequency, because the nonmotile state is not exerting force on the matrix. We expect that the other rate constants should decrease with increasing $\eta^2\omega^2$, which is consistent with our experimental data (Fig. 4*C*).

SI Text S4. Estimating the Undulation Frequency from the Power Dissipated by a Swimming Spirochete

B. burgdorferi is a long, thin organism with a length of 10–20 μm and a diameter of ~300 nm (6). The spirochete swims by propagating sinusoidal (or approximately sinusoidal) traveling waves down its length. In a fluid environment, the speed at which an undulating swimmer moves is dependent on the amplitude and wavelength of the waveform and the undulation frequency. The speed does not depend directly on the viscosity of the medium. In our experiments, we found that the concentration of gelatin in the environment affected the frequency of these traveling waves without altering the wave shape. In addition, the gelatin matrices behaved like a non-Newtonian fluid. To determine the effect of the non-Newtonian characteristic of the medium on swimming speed, we compared the swimming speed of the swimmer in gelatin to the speed of the equivalent swimmer (i.e., one with the same waveform and frequency) in a Newtonian fluid.

For long, thin swimmers in a Newtonian fluid at low Reynolds number, resistive force theory (RFT) is a fairly accurate method for computing the speed that a swimmer propagates, as long as the wavelength of the swimmer is much longer than the diameter of the cell body (7, 8). This method relates the local velocity of the centerline of the swimmer, $\mathbf{v}$, to the force per length that is exerted on the fluid, $\mathbf{f}$. There are two drag coefficients that determine the ratio of the force per length to the velocity. Motion perpendicular to the long axis of the swimmer has a ratio of force to velocity $\zeta_\perp$, which is the perpendicular drag coefficient. Motion along the tangent direction, $\hat{\mathbf{t}}$, has a ratio $\zeta_\parallel$ (the tangential drag coefficient). We can therefore relate the velocity to the force per length as

$$\zeta_\perp \mathbf{v} + (\zeta_\parallel - \zeta_\perp)(\mathbf{v}\cdot\hat{\mathbf{t}})\hat{\mathbf{t}} = \mathbf{f}. \quad \text{[S8]}$$

The ratio of the drag coefficients, which is important in determining the speed of the swimmer, has been computed to be (9)

$$\frac{\zeta_\perp}{\zeta_\parallel} \approx 2 - \frac{2}{\ln\left(\frac{2\lambda}{a}\right) - \frac{1}{2}}, \quad \text{[S9]}$$

where λ is the wavelength of the waveform and a is the radius of the cell body.

For a sinusoidal traveling wave aligned with the x axis, we can decompose the velocity into a constant translational velocity $\mathbf{U}_0$ plus a time-dependent sinusoidal velocity,

$$\mathbf{v} = \mathbf{U}_0 - \frac{A\omega}{2}\cos\left(\frac{2\pi x}{\lambda} - \omega t\right)\hat{\mathbf{y}}, \quad \text{[S10]}$$

where A is the amplitude of the waveform and ω is the frequency. The average translational velocity can be determined from the condition that the net force that the swimmer exerts on the fluid is equal to zero,

$$\int_0^L \mathbf{f}\,dx = 0, \quad \text{[S11]}$$

with the integral taken over the length of the swimmer. Calculations such as this were done previously in the context of spirochete locomotion (10). For the resistive force balance that we use here (Eq. **S8**), we find a velocity

$$\mathbf{U}_0 = \left(\frac{\lambda\omega}{2\pi}\right)\frac{\left(1-\frac{\zeta_\perp}{\zeta_\parallel}\right)\left(\frac{\pi^2A^2}{2\lambda^2}\right)}{\left(1+\frac{\zeta_\perp\pi^2A^2}{2\zeta_\parallel\lambda^2}\right)}\hat{\mathbf{x}}. \qquad \text{[S12]}$$

The term in the first bracket in Eq. **S12** is the wave speed of the undulation. The remaining terms are ∼0.1 for parameters relevant for *Bb*. Therefore, in liquid media, the swimming speed is ∼1/10th of the wave speed, as has been previously noted (11). When *Bb* swims without slipping, the swimming speed is equal to the wave speed. Therefore, the ratio of the "no-slip" swimming speed to the equivalent swimming speed in liquid is 10.

SI Text S5. Estimating the Undulation Frequency from the Power Dissipated by a Swimming Spirochete

The undulations of *Bb* that drive swimming are generated by the rotation of flagella that are located in the periplasmic space and are driven by flagellar motors. At low rotational speeds (less than a few hundred revolutions per second), the flagellar motor of a number of bacteria has been shown to produce a species-dependent, approximately constant torque (12, 13). Because *Bb* undulates at ∼10 Hz, we expect that we can treat the *Bb* flagellar motor as a constant torque motor that produces a torque τ_0. Therefore, the power that the flagellar motor inputs into motility is $\tau_0\omega$. If the average number of flagella per spirochete is N, then the total power input is $N\tau_0\omega$.

During swimming, the power that is supplied by the flagellar motor should be balanced by the power dissipated by swimming. Power is dissipated in two ways. First, we expect that rotation of the flagellum in the periplasmic space is resisted by a fluid dynamic torque, as was recently predicted from theoretical considerations (14). The power dissipated by rotating the flagella in the periplasmic space should be equal to $N\zeta_r L\omega^2$, where L is the length of the flagellum and ζ_r is a rotational drag coefficient. Second, movement of the cell body through the environment also dissipates energy. In our experiments, the external environment is a gel, which has a finite elastic modulus and an effective viscosity. A simple model for the force per length that is experienced by a filamentary swimmer undulating in a gel is one that considers the standard resistive force from the viscosity (Eq. **S8**) plus an elastic restoring force. Therefore, we assume that the force per length is given by

$$\mathbf{f} = \zeta_\perp\mathbf{v} + \left(\zeta_\parallel-\zeta_\perp\right)\left(\mathbf{v}\cdot\hat{\mathbf{t}}\right)\hat{\mathbf{t}} + \sigma_0\left((\mathbf{r}-\mathbf{r}_0)\cdot\hat{\mathbf{n}}\right)\hat{\mathbf{n}}, \qquad \text{[S13]}$$

where $\mathbf{r}_0$ is an initial deformation of the matrix, $\hat{\mathbf{n}}$ is the direction normal to the filament, and σ_0 is an elastic constant. The power dissipated is given by the integral of the dot product of $\mathbf{f}$ times $\mathbf{v}$ over the length of the bacterium. Because elastic forces do not dissipate energy, the last term on the right-hand side of Eq. **S13** does not contribute to the power. If we assume a sinusoidal traveling wave (as was done in *SI Text S4*), it is straightforward to show that the first-order contribution to the power dissipated by the swimmer in this simple model for swimming through a gel is

$$P_d = \zeta_r NL\omega^2 + \zeta_\parallel U_0^2 L + \frac{1}{8}\zeta_\perp A^2\omega^2 L + \frac{\pi^2}{2}\left(\zeta_\perp-\zeta_\parallel\right)\frac{U_0^2A^2L}{\lambda^2} + \frac{\pi}{2}\left(\zeta_\perp-\zeta_\parallel\right)\frac{U_0A^2\omega L}{\lambda}. \qquad \text{[S14]}$$

Balancing this power dissipated by the power input leads to an equation that defines the frequency. There are two cases that we need to consider. First, wriggling bacteria do not translocate; therefore $U_0 = 0$. For this case, we find

$$\left(\zeta_r NL + \frac{1}{8}\zeta_\perp A^2 L\right)\omega = N\tau_0. \qquad \text{[S15]}$$

We assume that the perpendicular drag coefficient should be proportional to the effective viscosity of the fluid and we define $\zeta_\perp = \zeta_0\eta$. Therefore, the inverse of the frequency should be a linear function of the viscosity:

$$\frac{N\tau_0}{\omega} = \left(\frac{\zeta_0A^2L}{8}\right)\eta + \zeta_r NL. \qquad \text{[S16]}$$

The second case we need to consider is one where the spirochete swims without slipping; (i.e., $U_0 = \lambda\omega/2\pi$). For this case, we find

$$\left(\zeta_r N + \frac{\zeta_\parallel\lambda^2}{4\pi^2} + \frac{1}{2}\left(\zeta_\perp - \frac{3}{4}\zeta_\parallel\right)A^2\right)L\omega = N\tau_0. \qquad \text{[S17]}$$

For *Bb* $\lambda/2\pi \sim A/2$; therefore

$$\frac{N\tau_0}{\omega} = \left(\zeta_\perp - \frac{1}{4}\zeta_\parallel\right)\frac{A^2L}{2} + \zeta_r NL. \qquad \text{[S18]}$$

In a viscous fluid, $\zeta_\parallel \approx \zeta_\perp/2$, and we can simplify this to

$$\frac{\tau_0}{\omega} = \left(\frac{7\zeta_0A^2L}{16}\right)\eta + \zeta_r L. \qquad \text{[S19]}$$

Note that the wriggling frequency (Eq. **S16**) and the translocating frequency (Eq. **S19**) have the same form. The only difference is that the prefactor that multiplies the viscosity for the translocating frequency is larger by a factor of 7/2 than the prefactor in the wriggling frequency. Therefore, we can write the inverse frequency for both of these cases using a single expression,

$$\frac{\tau_0}{\omega} = \alpha\left(\frac{\zeta_0A^2L}{8}\right)\eta + \zeta_r L, \qquad \text{[S20]}$$

where $\alpha = 1$ for wrigglers and 7/2 for translocators. We find very good agreement between our data and this expression. This result is surprising as it suggests that the undulation frequency depends only on the gel viscosity and not on the elasticity. In addition, it suggests that the resistive drag in a gel is similar to that in a viscous fluid and that the ratio of the perpendicular drag coefficient to the parallel drag coefficient is ∼2.

1. Zambrano MC, Beklemisheva AA, Bryksin AV, Newman SA, Cabello FC (2004) Borrelia burgdorferi binds to, invades, and colonizes native type I collagen lattices. *Infect Immun* 72:3138–3146.
2. Bockenstedt LK, et al. (1997) *Borrelia burgdorferi* strain-specific Osp C-mediated immunity in mice. *Infect Immun* 65:4661–4667.
3. Dunham-Ems SM, et al. (2009) Live imaging reveals a biphasic mode of dissemination of Borrelia burgdorferi within ticks. *J Clin Invest* 119:3652–3665.
4. Lancaster P, Salkauskas K (1981) Surfaces generated by moving least squares methods. *Math Comput* 37:141–158.
5. Bell GI (1978) Models for the specific adhesion of cells to cells. *Science* 200: 618–627.
6. Goldstein SF, Buttle KF, Charon NW (1996) Structural analysis of the Leptospiraceae and Borrelia burgdorferi by high-voltage electron microscopy. *J Bacteriol* 178: 6539–6545.
7. Yang J, Wolgemuth CW, Huber G (2009) Kinematics of the swimming of Spiroplasma. *Phys Rev Lett* 102:218102.
8. Jung S, Mareck K, Fauci L, Shelley MJ (2007) Rotational dynamics of a superhelix towed in a Stokes fluid. *Phys Fluids* 19:103105.
9. Cox RG (1970) The motion of long slender bodies in a viscous fluid Part 1. General theory. *J Fluid Mech* 44:791–810.
10. Chwang AT, Winet H, Wu TY (1974) A theoretical mechanism of spirochete locomotion. *J Mechanochem Cell Motil* 3:69–76.

11. Goldstein SF, Charon NW, Kreiling JA (1994) *Borrelia burgdorferi* swims with a planar waveform similar to that of eukaryotic flagella. *Proc Natl Acad Sci USA* 91:3433–3437.
12. Li G, Tang JX (2006) Low flagellar motor torque and high swimming efficiency of *Caulobacter crescentus* swarmer cells. *Biophys J* 91:2726–2734.
13. Chen X, Berg HC (2000) Torque-speed relationship of the flagellar rotary motor of *Escherichia coli*. *Biophys J* 78:1036–1041.
14. Yang J, Huber G, Wolgemuth CW (2011) Forces and torques on rotating spirochete flagella. *Phys Rev Lett* 107:268101.

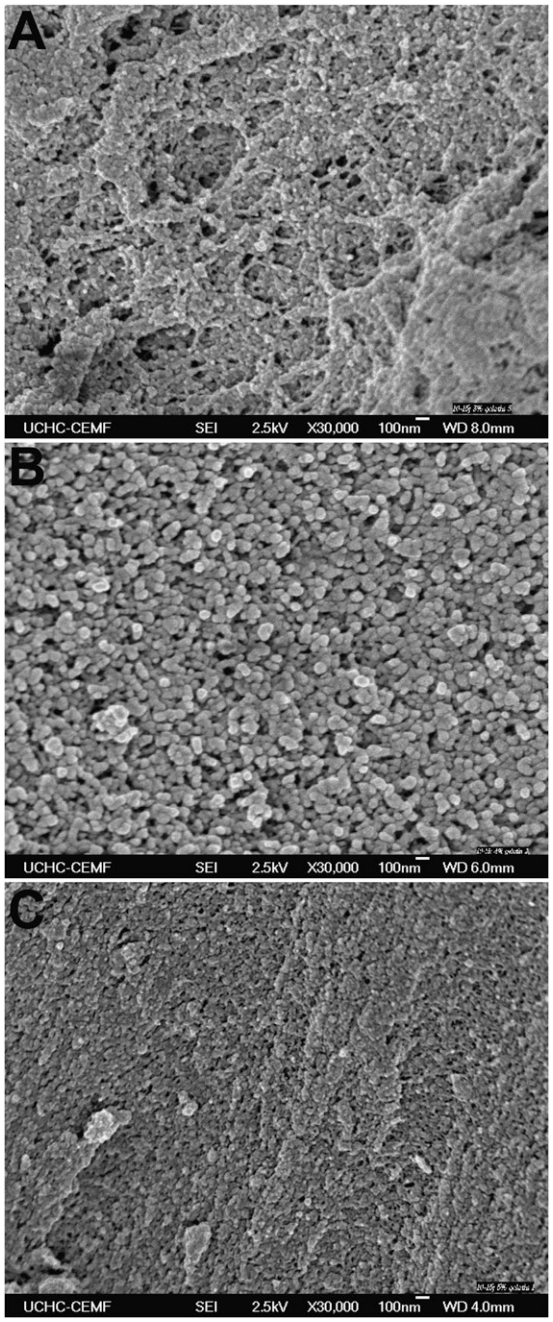

Fig. S1. Scanning electron microscope images of the 3% (*A*), 4% (*B*), and 5% (*C*) gelatin matrices.

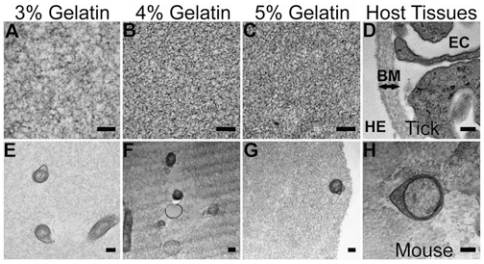

Fig. S2. (*A–C*) TEM images of gelatin matrices show that the pore size of the gelatin is much smaller than the cross-sectional diameter of a spirochete. (*D*) TEMs of a tick midgut, showing the midgut epithelial cells (EC), basement membrane (BM), and hemocoel (HE). The basement membrane structure is qualitatively similar to the gelatin matrices. (*E–G*) TEM images of *Bb* in 3–5% gelatin matrices. The gelatin is in intimate contact with the outer membranes of the bacteria and appears approximately uniform in density. (*H*) TEM image of *Bb* in the mouse dermis. The bacterium is surrounded by collagen fibers, which are in close contact with the bacterium. (Scale bars, 150 nm.)

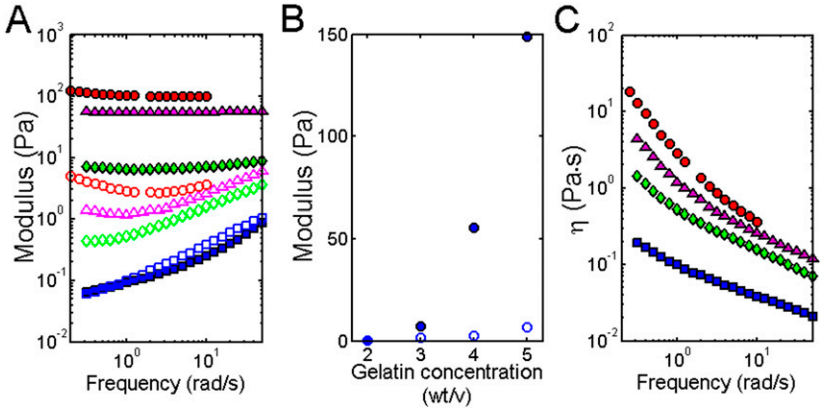

Fig. S3. (*A*) Rheology measurements of the gelatin matrices determine the complex moduli as a function of the angular frequency. The 3–5% gelatin matrices are gels with moduli of ~6 Pa (3%, green), 50 Pa (4%, magenta), and100 Pa (5%, red) and no significant contribution from viscosity at all accessible frequencies (the storage modulus, G', is shown as solid circles, and the loss modulus, G'', is shown as open circles). The 2% gelatin matrix is also a gel with a much smaller modulus that has significant contributions from viscosity at all frequencies (G', solid blue squares; G'', open blue squares). (*B*) The moduli at 10 rad/s as a function of gelatin concentration. G' is shown as solid circles, and G'' is shown as open circles. (*C*) The effective viscosity $\eta = G''/\omega$ as a function of the frequency. Blue circles, 2% gelatin; green diamonds, 3% gelatin; magenta triangles, 4% gelatin; and red circles, 5% gelatin.

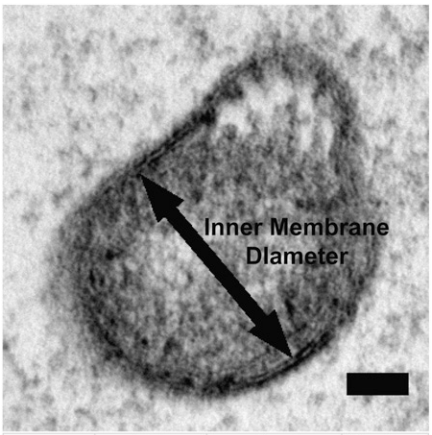

Media	Cells Measured (N)	Inner Membrane Diameter (nm)	Standard Error (nm)
BSKII	13	205	4.8
2% Gelatin	11	199	6.2
3% Gelatin	4	218	7.8
4% Gelatin	9	180	4.0
5% Gelatin	2	239	2.2

Fig. S4. The cross-sectional diameter of *B. burgdorferi* is not dependent on gelatin concentration. TEM image of a Bb914 cell in a 3% gelatin matrix is shown. (Scale bar, 50 nm.) We measured the cross-sectional diameters of the cytoplasmic cylinders of organisms in BSKII medium and in gelatin matrices. Using ImageJ, we fitted each cross-section with two perpendicular diameters, each representing the minor and major axes of the cell, and with a circle defined by three unique points selected along the inner membrane. These three measurements were then averaged to define the diameter of each bacterium. The table shows cell diameter as a function of gelatin concentration. Comparison of the mean diameters for the different gelatin concentrations revealed no statistically significant differences.

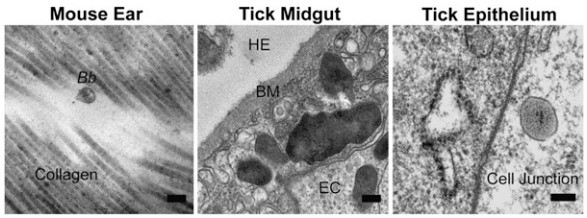

Fig. S5. TEM images of the dermis of a mouse (*Left*), tick midgut (*Center*), and a cell junction between two tick midgut epithelial cells (*Right*). (*Left*) Bb914 in the dermis of the mouse. The collagen fibers form a dense striated pattern. The bright region in the center of the image could be an artifact or a void in the collagen network. The bacterium (*Bb*) is observed to be near to and possibly within the dense array of collagen. (*Center*) The basement membrane (BM) appears similar to the gelatin matrix system. Also shown are a midgut epithelial cell (EC) and the hemocoel (HE). (*Right*) The junction between midgut epithelial cells is extremely narrow. Spirochetes must penetrate through junctions such as these to reach the basement membrane. (Scale bars, 150 nm.)

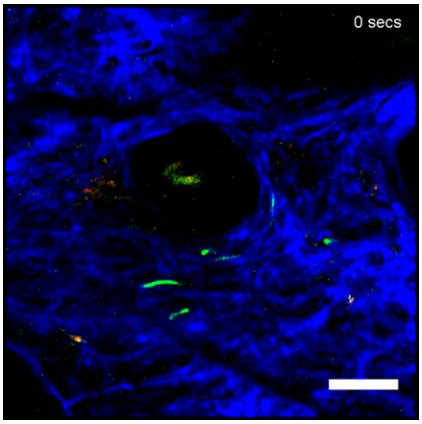

Movie S1. The motility of *B. burgdorferi* in the dermis of the mouse at 98 d of infection. This time-lapse movie of Bb914 in the ear of a tick-inoculated wild-type mouse demonstrates lunging, wriggling, and translocating bacteria in the dermis. The movie corresponds with the time sequence shown in Fig. 1*A*. (Scale bar, 50 μm.)

Movie S1

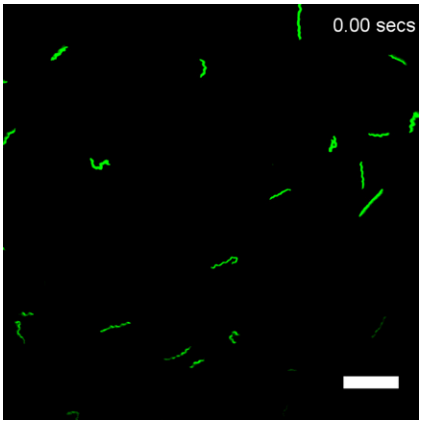

Movie S2. The motility of Bb914 in a 3% gelatin matrix. This time-lapse movie uses live-imaging confocal microscopy to demonstrate the four motility states defined in the text. The movie corresponds with the time sequence shown in Fig. 1*B*. The time interval between frames is 1 s. (Scale bar, 30 μm.)

Movie S2

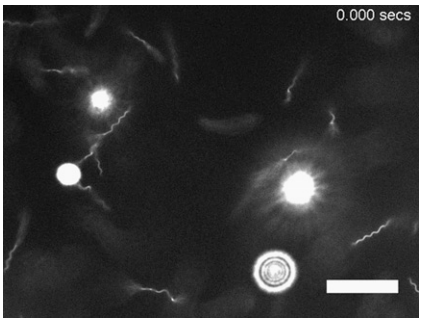

Movie S3. Bb914 in BSKII medium with 500-nm diameter fluorescent microspheres. The spheres show large displacement due to Brownian motion. (Scale bar, 20 μm.)

Movie S3

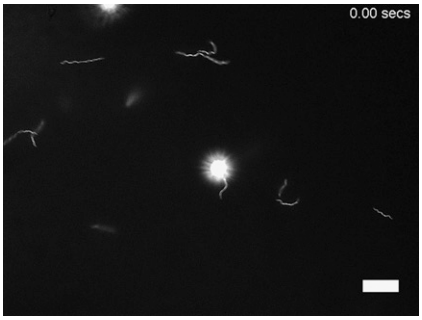

Movie S4. Bb914 in a 3% gelatin matrix with 500-nm diameter fluorescent microspheres. The spheres are nearly stationary, confirming that both spheres and bacteria are inside the gelatin matrix. (Scale bar, 20 μm.)

Movie S4

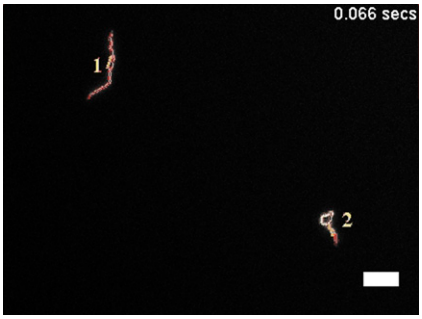

Movie S5. The output of our tracking algorithm. Two spirochetes are shown. The contours that the tracking algorithm determines for the centerline of each spirochete are drawn in red. Tan lines depict the average orientation of each spirochete. The algorithm also labels each spirochete with a number. (Scale bar, 10 μm.)

Movie S5

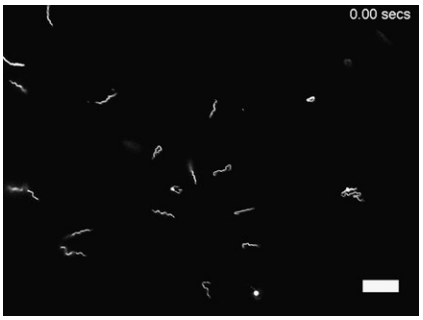

Movie S6. The motility of *B. burgdorferi* in a 2% gelatin matrix. This movie shows high-speed epifluorescence microscopy of Bb914 and demonstrates the four motility states that we define in the text. The movie corresponds with the time sequence shown in Fig. 2*A*. The time interval between frames is 1 s. (Scale bar, 20 μm.)

Movie S6

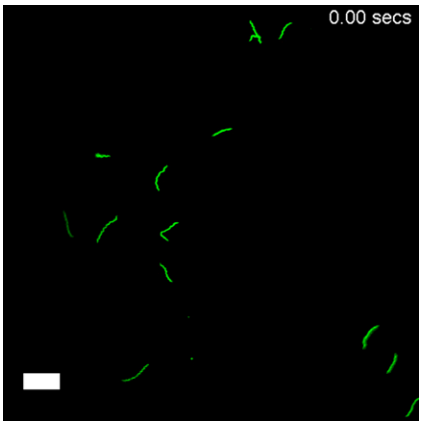

Movie S7. Confocal microscopy of Bb914 in a 3% gelatin matrix, demonstrating borrelial motility on a longer timescale (5 min). The movie corresponds with the time sequence shown in Fig. 4*A*. (Scale bar, 20 μm.)

Movie S7